Optimizing UAV Aerodynamics with Computational Fluid Dynamics

João Nuno Dias Carvalho
joao.nuno.dias.carvalho@tecnico.ulisboa.pt

Instituto Superior Técnico, Universidade de Lisboa, Portugal

December 2016

Abstract

The purpose of this paper is to employ low subsonic aerodynamic theories, through CFD analysis, to optimize the main wing of a MALE UAV and achieve an increase in performance superior to 10%. The configuration for the MALE UAV was provided by the Portuguese Air Force and an analysis with the RANS equations, the Menter SST $k-\omega$ and the $\gamma - Re_\theta$ models, at a Mach number of 0.2 and a Reynolds number of 2.2×10^6, is performed in order to evaluate the integral coefficients. To determine the influence of the design parameters of wing tip devices, a sensibility study in a 3D panel method is employed and confirmation of the results is done by analyzing the best configurations with simulations in RANS. A grid refinement study is then executed to ensure accuracy of the increases and estimate the exact numerical values for the engineering quantities. Results show that the panel method fails to achieve the desired precision in predicting the increases in performance but allows a qualitative insight on the influence of the design parameters. RANS simulations determine a 20% increase in L/D and a 30% increase in $C_L^{3/2}/C_D$ from the cut-off configuration.

Keywords: Unmanned Aerial Vehicles, External Aerodynamics, Computational Fluid Dynamics, Wing Tip Devices, Sensitivity Study

1. Introduction

According to TEAL Group Corporation, the development in Unmanned Aerial Vehicles (UAV) in the twenty-first century has been the most dynamic area within the entire aerospace industry. The recent demand enforces manufacturers and their operating partners to maximize the performance of such platforms. From the aerodynamic point of view, this maximization of performance is achieved by reducing drag and attentions have been directed towards the reduction of wing tip vorticity and therefore lift-induce drag. [1]

The physics of the wing tip vortex in the near-field is extremely complex as it is a three-dimensional and turbulent phenomena. Due to the pressure difference between the upper and lower surface of the wing, a strong cross-flow is induced and a wing tip vortex is formed. [2] The inclusion of wing tip devices has proven beneficial in reducing this pressure gradient in airliners at high subsonic applications and is now target of several studies to determine the effects in low subsonic flows.

As described by Maughmer [3], early attempts on evaluating the influence of design parameters of winglets for low subsonic applications, at the Pennsylvania State University, were performed using trial-and-error approaches using flight testing. Ning and Kroo [4], at Stanford University, have used multidisciplinary optimization techniques to determine the effects of several tip designs and, in 2014, Panagiotou et al. [5] performed parametric studies of the design parameters of winglets for a Medium-Altitude Long-Endurance Unmanned Aerial Vehicles (MALE UAV) for the Hellenic Air Force.

Following this line of studies, this paper integrates a broader set of activities developed by the Portuguese Air Force, in collaboration with Instituto Superior Técnico, for the construction and optimization of a MALE UAV prototype. Aiming at maximizing the performance of this platform, this paper sets out to explore the aerodynamic design of wing tip devices with Computational Fluid Dynamics (CFD) tools in order to increase range and endurance in, at least, 10%.

2. Theoretical Background

Endurance and range are two concepts that, quite often, are misused and create confusion. While endurance can be defined as the maximum time, range is the maximum distance an aircraft is airborne un-

der a certain flight condition without being refueled. [6] These concepts can be mathematically defined with the Breguet equations, commonly found in the imperial unit system. These show that, for propeller-driven aircrafts, range depends on L/D ratio, whilst endurance depends on $C_L^{3/2}/C_D$. Since both performance coefficients depend on lift and drag, maximizing them can be done wither by increasing lift or decreasing drag. The current paper focuses on the second objective. [7]

The total drag of an airplane is frequently divided in two components, parasite drag and lift-induced drag. The parasite drag is all the drag that does not appear from the creation of lift and the vorticity shed into the wake. It contains the friction/form, interference and wake drag. The lift-induced drag, as the name suggests is the drag that is a result of the vorticity shed into the wake. [8] Even though parasite drag accounts for a very large part of the total aircraft drag, its reduction is the most difficult to accomplish and, in this paper, efforts will only be spent in reducing lift-induced drag.

In fact, reducing drag of this nature can be achieved through the reduction in the intensity of the wing tip vortex. The concept of eliminating all trailing vorticity was first conceived by Lanchester in 1897 when he proposed the inclusion of wing endplates. [9] Following Lanchester's theories, Whitcomb [10] developed the first winglet predicting that the lift-to-drag ratio would increase in about 9%.

Attempts on providing interpretations to the results of Lanchester and Whitcomb was proposed by Gudmundsson [11]. In his interpretation, the shape of the wing tip distorts the flow field around the wing, pushing the wing tip vortex closer or further away from the symmetry plane. This fact explains the reason why a cut-off wing has better performance than a round tip wing. The reduction witnessed in lift-induced drag with the inclusion of winglets and raked tips may be interpreted as an increase in aspect ratio created by the translation of the vortex outward. The final drag coefficient is then computed with the following equation.

$$C_D = C_{D_0} + \frac{C_L^2}{\pi \cdot (AR + \Delta AR) \cdot e} \tag{1}$$

Results obtained by Gudmundsson [11] with the potential flow theory show that the winglet and the raked tip are the most efficient wing tip devices when reducing lift-induced drag.

Span extensions, winglets and C-wings were tested by Ning and Kroo [12] and results show that, for negative and zero pitching moments, C-wings and winglets present a similar drag reduction with winglets being slightly more efficient. For positive moments about the aerodynamic center, C-wings produce better results.

In very recent studies, it has been proven that an optimized blended winglet in low subsonic flights can increase the lift-to-drag ratio up to 16%. This geometry is shown bellow in figure 1.

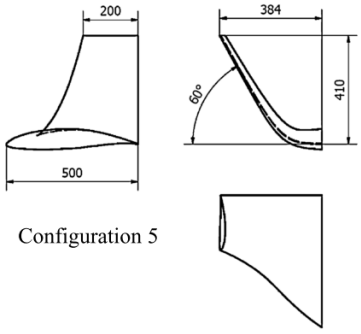

Figure 1: Schematics for a blended winglet. [5]

3. Mathematical Models

The physics of the airflow around an aircraft is a complex problem and an algebraic solution is achievable only for a very limited amount of scenarios. Two groups of mathematical models are used in this paper, surface and volume models. The surface model employed is the aerodynamic potential-flow code, commonly known as panel method. The method based on the finite volume formulation are the Reynolds-Averaged Navier-Stokes (RANS) equations. A detailed description of these two models is provided in next subsections.

3.1. Panel Method

Deriving from the equation of conservation of mass, the panel method is extremely useful when performing simple flow analysis on complex geometries. This method is often used when the flow can be approximated by an inviscid and incompressible potential flow, providing results that are in agreement with experimental results. [13]

$$\left(1 - M_\infty^2\right) \phi_{xx} + \phi_{yy} + \phi_{zz} = 0 \tag{2}$$

From the Prandtl-Glauert equation for small disturbances (equation 2), the panel method converts into an integral equation for the potential of the flow using Green's theorem (equation 3). [13]

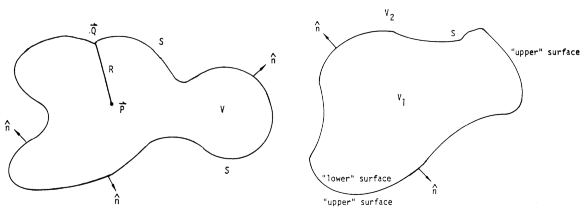

Figure 2: Generic control volumes used in the discretization of the panel method.

If the generic control volumes present in figure 2 are used in the discretization of the Prandtl-Glauert equation, one can arrive to the equation 3 for the potential of the flow. [13]

$$\phi(P) = -\frac{1}{4\pi}\iint_S \left[\frac{\hat{n}\cdot(\nabla\phi_U - \nabla\phi_L)}{R} - \right. \\ \left. -(\phi_U - \phi_L)\cdot\hat{n}\cdot\nabla\frac{1}{R}\right] dS_Q \quad (3)$$

Equation 3 is applied to 2D quadrilateral panels, resultant of the discretization process, that cover both the aircraft and its wake. Since the panel method only discretizes the geometry, it is less resource consuming than the mathematical models present in subsequent sections.[13]

3.2. Reynolds-Averaged Navier-Stokes – RANS

The RANS equations are obtained through the Reynolds-averaged method, by assuming all unsteadiness in the Navier-Stokes equations is averaged. This is done by considering that the value of a property is the sum of the mean value and a fluctuation around it. Time-averaging is the common approach for achieving the RANS equations, however, if the unsteady RANS equations are to be achieved, time-averaging is not an option and the ensemble-averaging approach must be used. This process results in the averaged equations of continuity and momentum, present in equations 4a and 4b, in tensor notation. [14]

$$\frac{\partial(\rho\overline{u}_i)}{\partial x_i} = 0 \quad (4a)$$

$$\frac{\partial(\rho\overline{u}_i)}{\partial t} + \frac{\partial}{\partial x_j}\left(\rho\overline{u}_i\overline{u}_j + \rho\overline{u_i'u_j'}\right) = -\frac{\partial\overline{p}}{\partial x_i} + \\ + \frac{\partial}{\partial x_j}\left[\mu\left(\frac{\partial\overline{u}_i}{\partial x_j} + \frac{\partial\overline{u}_j}{\partial x_i}\right)\right] \quad (4b)$$

Due to additional terms that are created with the averaging of the equations, turbulence models are needed to create a closed system of equations. [14]

For external CFD analysis with airfoils, the turbulence models that provide acceptable predictions of the flow are the Spalart-Allmaras and the Menter SST $k-\omega$ models.

The Spalart-Allmaras is a turbulence model specially designed for aeronautical cases. Weaknesses in the Spalart-Allmaras model have been witnessed in flows with massive separations, wakes with pressure gradients and free vortices. [15] This turbulence model is a one-equation model that couples, to the RANS equations, a partial differential equation for the kinematic eddy-viscosity parameter, $\tilde{\nu}$. The Menter SST $k-\omega$ is a variation of the Willcox $k-\omega$ and the $k-\varepsilon$. This model employs the $k-\omega$ proposed by Willcox near solid walls and takes advantage of the robustness of the $k-\varepsilon$ model in the free-shear flow. [16] Since the flow is likely to have both turbulent and laminar regions, transition has to be modeled. For this reason, the turbulence model employed in this paper is the Menter SST $k-\omega$ coupled with the $\gamma - Re_\theta$ transition model. This combination of models has been tested in several aeronautical cases and the results are in agreement with the available experimental results. Prediction of laminar separation bubbles and other separations can be achieved with this model. [17]

For this reason the turbulence and transitions models chosen for implementation on this paper are the Menter SST $k-\omega$ and the $\gamma - Re_\theta$ models.

4. Initial Configuration

The UAV provided by the Portuguese Air Force is a propeller driven aircraft and has a twin-boom pusher configuration, which is common for MALE UAVs. It is possible to see the provided geometry in figure 3. The given aircraft couldn't be directly used in a CFD software, since softwares of such nature require more detail than Computer Aided Design (CAD) softwares. Therefore, before importing in STAR-CCM+, it was necessary to model the geometry in a CAD software and perform further operations in STAR-CCM+.

In order to simplify the problem and reduce the computational effort and time spent on a CFD analysis, the front landing gear and the rear section of the fuselage had to be intervened. Even though the CFD software can perform an analysis with the original geometry, these simplifications reduce the mesh size with no considerable influence in the dynamics of the flow or the integral coefficients. With the geometry simplified, it was necessary to prepare it the for the meshing process. In order to be able to mesh and simulate, it is necessary to create a closed region with no self-intersecting faces. For this effect, the Surface Wrapper operation was performed in STAR-CCM+.

In order to solve the RANS equations, the control volume needs to be discretized. For this purpose one of three possible mesh types (structured, block-structured and unstructured) needs to be employed. Most modern CFD codes solve all meshes as unstructured, even if they are structured or block-structured, keeping the connectivity matrix and solving the equations using this matrix to determine the neighbors of each cell. On the other hand, structured meshes can only be achieved for simple geometries which are rarely found in real life applications. Block-structured and unstructured meshes can be composed of tetrahedral, trimmed or polyhedral cells. Prismatic layers are added in order to better predict the behavior of boundary layers near

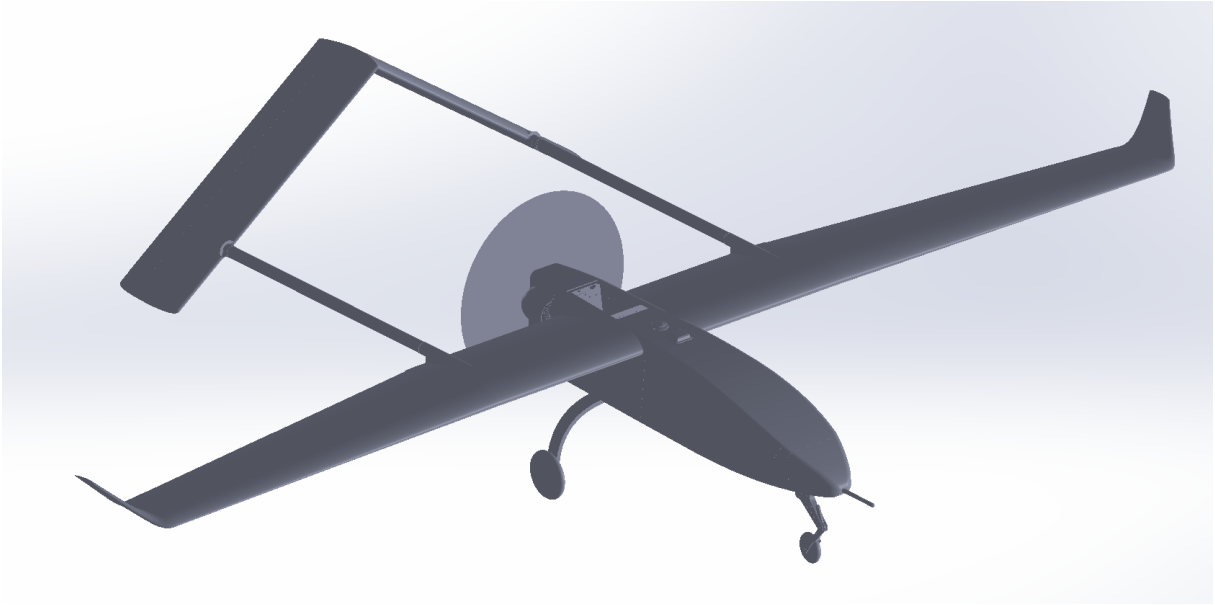

Figure 3: Initial configuration provided by the Portuguese Air Force

solid walls.

To begin with, the best practice guidelines, provided by Veríssimo [18], were followed and the trimmed meshing code coupled with prismatic layers were employed. The base size defined was equal to one chord (main wing) and, in order, to capture certain details of the geometry and fluid phenomena, it was necessary to use volumetric control refinements throughout the domain. Inside these refinements, the target size of the cells was adjusted and defined as a percentage of the base size.

The final mesh had 21.7 million cells and a trimmed mesh with about 20 million cells should provide good results for this application and ensure that the solution for the integral coefficients show deviations to the exact numerical solution of less than 3%. [18]

With a Mach number of $M = 0.2$ and a Reynolds number of $Re_c = 2.2 \times 10^6$, at the altitude of 1500m the flow is considered incompressible and has a Reynolds number above $\sqrt{Re_x} = 1000$, the number at which the flow is likely to be turbulent. [19] In fact, for this Reynolds number, the flow is not entirely turbulent and transition from laminar to turbulent has an important role in predicting the flow.

As stated in section 3, the mathematical models employed in this paper are the RANS equations, coupled with the Menter SST $k-\omega$ turbulence model and the $\gamma - Re_\theta$ transition model, solved with the segregated flow solver. This transition model requires the definition of a free-stream edge and the value employed was equal to four times the maximum boundary layer thickness.

The domain was divided into 4 boundary types and the respective conditions applied to each type of boundary. The surface of the UAV, aligned with the flow ($\alpha = 0°$), was considered a no-slip wall and low y+ wall treatment was chosen, with a maximum y+ of 0.25. The upwind and lateral faces of the domain were considered just one boundary and the condition applied was of velocity inlet. In this case, the velocity magnitude and direction of cruise flight were prescribed. The velocity was of 68.33 m/s and was aligned with the x-direction. Turbulence was also specified in this boundary through its intensity and viscosity ratio. Values for these parameters of 0.1% and 1, respectively, were imposed. The symmetry plane was defined with the boundary condition of the same name and the downwind face considered a pressure outlet.

A recommendation from Veríssimo [18] suggests that the ambient source term of turbulence should be turned on and the turbulence intensity and viscosity ratio should be prescribed. The values used for the ambient source term were the same as the inlet, 0.1% for turbulence intensity and 1 for TVR.

The simulation was stopped when the residuals lowered their values down to $10^{-4}/10^{-5}$, with the exception of the turbulent kinetic energy that stabilized at 10^{-2}. The lift and drag coefficients and the lift-to-drag ratio converged in the fourth significant digit. The results of the values of interest are presented in table 1.

Even though results are within the predicted range, a few geometry related complications were found. By inspection of the pressure and skin friction distributions (suction side), for a section of the

C_L	C_D	L/D	$C_L^{3/2}/C_D$
0.3078	0.02310	13.32	7.392

Table 1: Results for the aerodynamic coefficients for the initial configuration.

main wing ($x/(b/2) = 74.4\%$), it is possible to verify the existence of oscillations in the same locations due to the lack of smoothness in the geometry. In fact, these oscillations are the result of a series of separations and reattachments created by sharp variations in the airfoil's geometry.

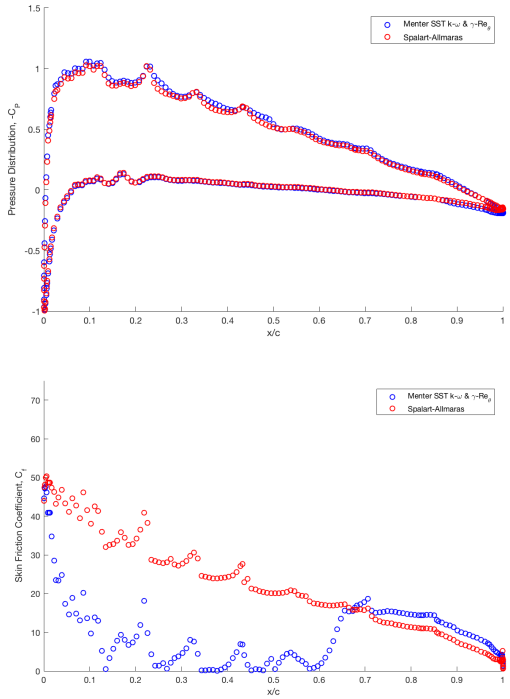

Figure 4: Pressure distributions (top) and skin friction coefficient distributions (bottom) computed with the Menter SST $k-\omega$ and the $\gamma - Re_\theta$ models (blue) and the Spalart-Allmaras model (red).

This conclusion was achieved by performing simulations with the Spalart-Allmaras turbulence model and observing the presence of the oscillations in the exact same positions. It is possible to confirm the statement presented in section 3 that this model assumes a fully turbulent flow from the beginning, thus not modeling the transition.

Overall, the current mesh was able to capture the wakes from the fuselage, rear landing gear and wing tip device until they almost diffused completely. It is important to keep in mind that the purpose of this mesh was to achieve convergence of the aerodynamic coefficients to a value that approached reality with small deviations from the exact numerical values. In this sense, the current mesh achieved the purpose and rendered acceptable values.

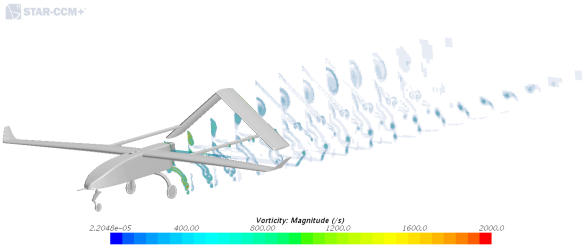

Figure 5: Visualization of the streamwise vorticity contours in the wake of the aircraft.

5. Wing Tip Device Study

Following the results presented by Gudmundsson [11], there was the need to explore the design of winglets and raked tips. For this task, the open source panel method software XFLR5 was employed and the internal CAD tool had to be used to design the initial configuration.

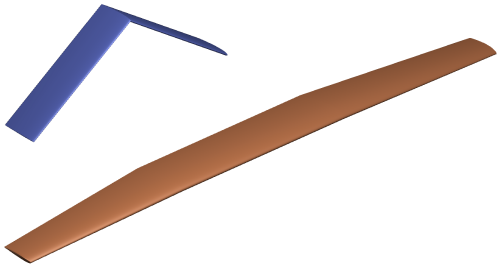

Figure 6: Reference wing-tail pair in XFLR5.

All the simulations in XFLR5 were performed solely with the wing and tail, and all the increments in the performance coefficients were determined with the reference wing-tail pair shown in figure 6. In fact, an attempt on simulating with the fuselage was done and the results were far from reality. In this simulation, XFLR5 created a vortex in the wing root, that should be resultant of the intersection with the fuselage. Since the fuselage is creating a very small amount of lift and no drag, the section occupied by this body could be, in fact, considered as empty. As a result, the wing/fuselage intersection vortex is being over-dimensioned, rendering unrealistic values for drag.

To be able to compare results from the panel method with the solution from STAR-CCM+, the parasite drag was calculated recurring to empirical formulas presented by Corke [19]. These formulas estimate the base drag of the wings, assuming they behave in the same way as flat plates with minimum amount of flow separations. In this case, the

base drag can be related to the skin friction coefficient multiplied by form factors to account for the imperfections in the flow. As for the fuselage, the drag estimated by the formulas is being calculated with the skin friction coefficient. The calculations present in Corke [19] are empirical formulas based in the skin friction drag and can be considered a low level drag estimation.

5.1. Sensitivity Study

As stated by Gudmundsson [11], the design parameters for winglets and raked tips are the same. These parameters are six and five of them (span, tip chord, sweep angle, dihedral angle and twist angle) could be analyzed in this sensitivity study. The last parameter, the blending radius couldn't be included in this analysis since it influences interference drag and XFLR5 does not evaluate viscous drag. The list of parameter variations was compiled in a single text file, with each line containing five values separated by spaces.

A macro was then created, in order to test the several design parameters. It ran for 1024 cycles, corresponding to the total number of combinations of 4 variations of the 5 parameters. After 51.2 hours, 1024 text files with the lift and drag coefficients of each configuration and respective simulation were created. At last a code in MATLAB was developed in order to analyze the data from the sensitivity study.

The variations in the design parameters, for the winglet, are presented bellow.

Span (m)	0.100, 0.200, 0.300, 0.400;
Tip chord (m)	0.100, 0.150, 0.200, 0.250;
Sweep angle (°)	0.0, 20.0, 40.0, 60.0;
Dihedral angle (°)	30.0, 40.0, 50.0, 60.0;
Twist angle (°)	0.0, 1.0, 2.0, 3.0;

Influence of the design parameters were created using MATLAB's Statistics and Machine Learning toolbox. Two plots are presented, the main effects plot and the interaction plot. The main effects plot depicts the average L/D ratio for each parameter variation. In other words, when given the list of input parameters and output solutions, MATLAB searches the entries with the same parameter variation and calculates the average value for the solution. It then plots the averaged value in each point of the graphic. The main effects plots can be seen in figures 7 and 8.

Figure 7 is extremely relevant to determine which design parameters have the largest influence in the L/D. Therefore, it is possible to conclude that the design parameters with the most influence in the L/D ratio are the span, followed by the sweep and dihedral. It is interesting to note that not all winglet designs present an increase in performance parameters, since the value of L/D can achieve values lower than the cut-off configuration, hence the importance of this work.

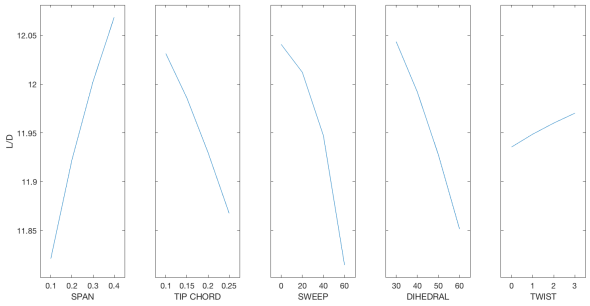

Figure 7: Influence of each design parameter in the objective function L/D - Winglet.

For the case of the raked tip, the parameter variations are presented bellow.

Span (m)	0.100, 0.200, 0.300, 0.400;
Tip chord (m)	0.050, 0.075, 0.100, 0.125;
Sweep angle (°)	0.0, 20.0, 40.0, 60.0;
Dihedral angle (°)	0.0, 2.5, 5.0, 7.5;
Twist angle (°)	0.0, 1.0, 2.0, 3.0;

Figure 8 shows the main effects plot for the results obtained with the raked tip.

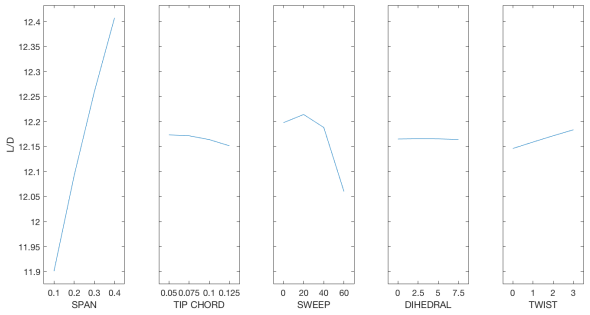

Figure 8: Influence of each design parameter in the objective function L/D - Raked Tip.

Figures 9 and 10 are common results of any sensitivity study. Known as interaction plots, they depict the objective function, in this case the L/D ratio, as a function of the interactions between the design parameters. These plots follow the same approach as the main effects plot and average the multiple possibilities for the objective function that fit in each point. Therefore, it is important to understand that in each column of this matrix of graphics, a specific design parameter is considered a variable and in each line is considered a constant, e. g. if one is analyzing the graphic in position (2,3), he or

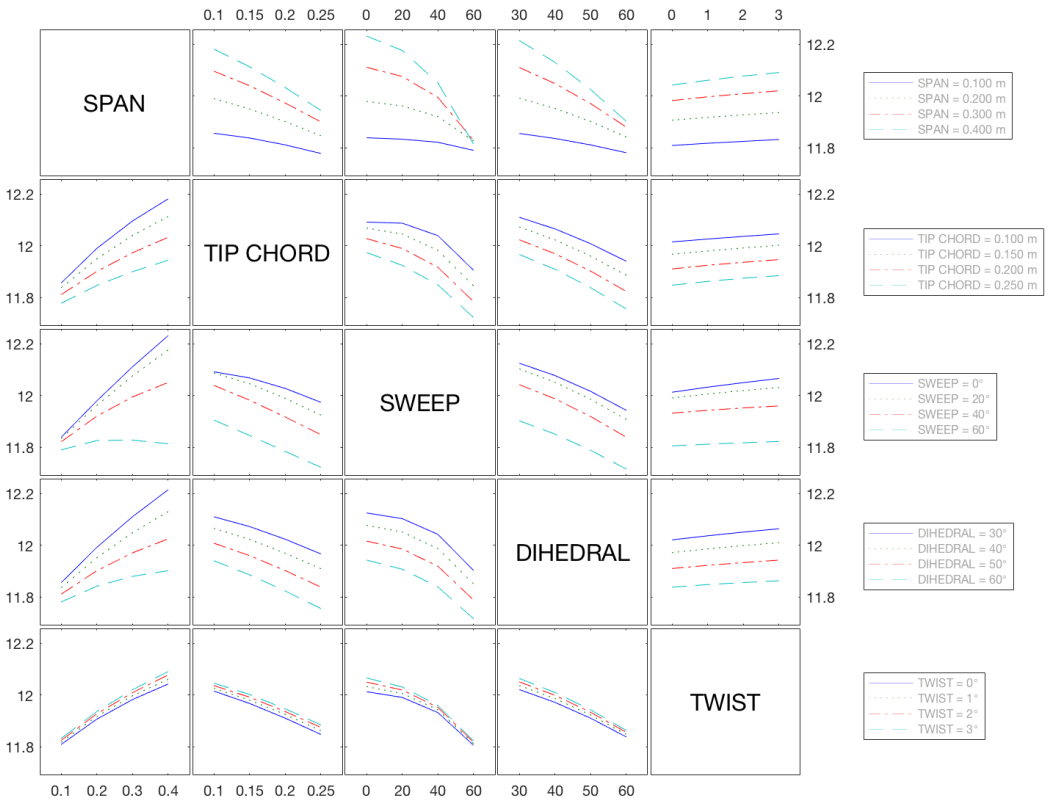

Figure 9: Interaction plot for L/D - Winglet.

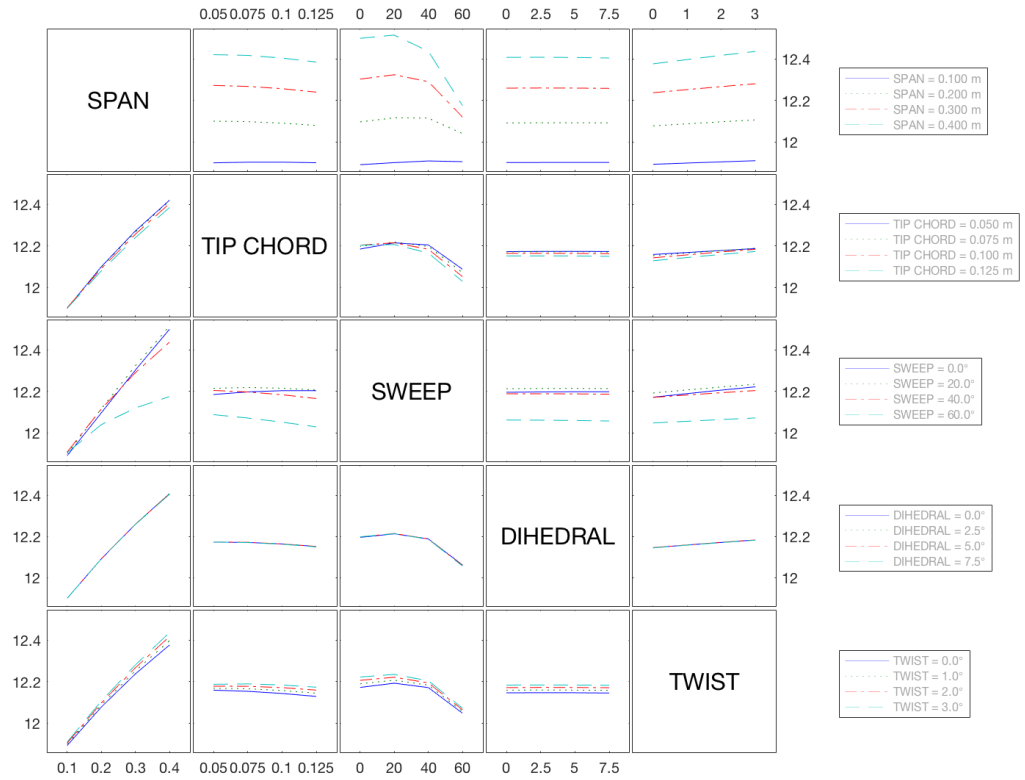

Figure 10: Interaction plot for L/D - Raked Tip.

she is looking at the value of L/D when the tip chord is considered constant and the sweep angle variable. For each point in this specific plot (2,3) there are several values for L/D since the rest of the parameters are changing. The value plotted is the average of all the possibilities.

As expected, the increase in span renders a substantial increase in the performance coefficients, since the results for $C_L^{3/2}/C_D$ show the same variations as L/D, with the only difference being in its value. The main reason for this result is the fact that by employing a wing tip device, one is increasing the effective aspect ratio and consequently increasing lift and decreasing lift-induced drag. With no surprises, with the increase in sweep angle there is a decrease in the performance coefficients. For low subsonic applications, including sweep only decreases the effective aspect ratio, increasing the lift-induced drag and decreasing L/D and $C_L^{3/2}/C_D$. In these cases, including sweep might be done for stability and control purposes or for aesthetic reasons. As for the dihedral angle, smaller values are preferable, since they mean the winglet is more horizontal, making, thus, lift more vertical.

The best combinations for the design parameters of both wing tip devices are presented bellow in table .

Span	Tip Chord	Sweep	Dihedral	Twist
0.400 m	0.100 m	0.0º	30.0º	3.0º

Table 2: Best combination of the winglet design parameters.

Span	Tip Chord	Sweep	Dihedral	Twist
0.400 m	0.075 m	20.0º	2.5º	3.0º

Table 3: Best combination of the raked tip design parameters.

As stated by Gudmundsson in is work [11], raked tips display slightly better performance coefficients than winglets. The same tendency was observed in this paper. The best raked tip presented in table 3 increases L/D and $C_L^{3/2}/C_D$ in 5.90% and 9.81%, respectively, while the best winglet (table 2) only increases 5.14% and 8.73%.

5.2. Confirmation with RANS Equations

In order to confirm the results from the sensitivity study, the winglet present in the initial configuration was either completely removed or replaced by the best configurations for winglet and raked tip from the sensitivity study. The configurations were analyzed with the same procedure as the initial configuration and in section 6, the best of the two wing tip devices and the cut-off configuration are target of a grid refinement study in order to guarantee that the obtained increases are numerically accurate.

The results showed that the tendency to prefer raked tips over winglets determined with the panel method is not confirmed by the RANS equations. In fact, wing tip streamwise vorticity plots showed that the winglet was diffusing and decreasing the intensity of the vortex, while the raked tip was just diffusing the vorticity, hence the lack of decrease in the drag coefficient.

The comparison of the increases obtained for the winglet are shown in table 4.

Simulation	$\Delta L/D$	Deviation	$\Delta C_L^{3/2}/C_D$	Deviation
XFLR5	5.14%	-74.39%	8.73%	-69.99%
STAR-CCM+	20.07%		29.09%	

Table 4: Comparison of the increases created by the winglet in XFLR5 and STAR-CCM+.

Deviations between the increases predicted with both methods, presented in table 4, were expected. In fact, the panel method only evaluates a portion of pressure drag, the lift-induced drag. On the other hand, the RANS equations are able to compute the totality of drag. The deviations of the XFLR5 towards the values obtained with STAR-CCM+ are considerable due to the fact that the method cannot predict a large amount of drag that is also being influenced by the inclusion of a wing tip device.

It's important to state that the results from STAR-CCM+ are in conformity with the results obtained by Panagiotou et al. [5], where the inclusion of winglets increased the L/D in 16% for a null angle of attack and 19% for a four degrees angle of attack. In the mentioned paper, the numerical models are equal to the ones used in this Thesis with the exception of the turbulence and transition models. Instead of using the Menter SST $k-\omega$ and the $\gamma-Re_\theta$ models, Panagiotou et al. employed the Spalart-Allmaras turbulence model. The fact that the results of this Thesis are in conformity with a paper with a different turbulence model enforces that the tendency to increase performance with winglets is not derived from a numerical model but is instead due to physical phenomena.

The comparison of the increases obtained for the raked tip are shown in table 5, where deviations of the same magnitude of the winglet can be found.

Simulation	$\Delta L/D$	Deviation	$\Delta C_L^{3/2}/C_D$	Deviation
XFLR5	5.90%	-58.51%	9.81%	-61.89%
STAR-CCM+	14.22%		25.74%	

Table 5: Comparison of the increase created by the raked tip in XFLR5 and STAR-CCM+.

The configurations that are target of a sensitivity

study in the next chapter are the cut-off and the winglet configurations.

6. Grid Refinement Study

Reliability and accuracy are two concepts frequently confused. In the context of CFD applications, reliability is associated with the robustness of the computational method employed and, therefore, the evaluation of iterative errors. Accuracy is composed of two types, the modeling and the numerical accuracy. The first is associated with the measure of the error created by the modeling of the physics by a certain mathematical model. The last can be described as the error generated by the discretization of the control volume.

The objective of this study is indeed to estimate the exact numerical solution for the engineering quantities and compute the uncertainty associated with the increases predicted in section 5.

The current study involves three unstructured finite volume meshes: a coarse, an intermediate and a thin mesh. The meshes employed in section 5 were considered the coarse meshes for the study and successive refinements were performed to arrive to the remaining meshes. These were achieved by successively decreasing the cell base size until the number of cells was near the target value. The base sizes that accomplished these meshes were, respectively, 0.350m and 0.271m.

The estimation for the exact numerical solution is obtain through the method proposed by Roache [20], where the value is computed using the Richardson Extrapolation. This method of computing the uncertainty of the engineering quantity was applied to the cut-off configuration. The estimations for the exact numerical solution of the lift and drag coefficients were 0.288065 and 0.023606, respectively. Figure 11 shows the values computed for the aerodynamic coefficients for the cut-off configuration (blue) and the Richardson Extrapolation (black), plotted against the grid refinement number, $r_i = \sqrt{h_f/h_i}$, where h_f is the number of cells of the thin mesh and h_i the number of cells of the intended mesh.

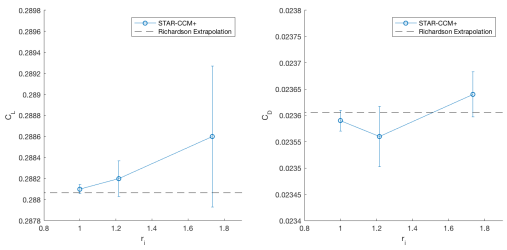

Figure 11: Grid convergence plots for the cut-off configuration.

Unlike in the case of the lift coefficient, figure 11 shows an increased difficulty in converging the drag coefficient.

For the case of the winglet, the estimation of the exact numerical values rendered values of 0.334994 and 0.022757 for the lift and drag coefficients, respectively. Figure 12 shows the convergence of both aerodynamic coefficients.

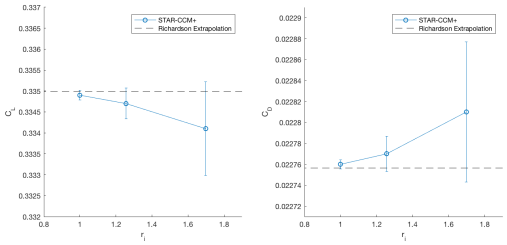

Figure 12: Grid convergence plots for the winglet configuration.

A comparison of the increases for the performances coefficients show deviations around 3% of the exact numerical value, confirming the accuracy of the solutions determined in section 5.

Solution	$\Delta L/D$	Deviation	$\Delta C_L^{3/2}/C_D$	Deviation
Coarse Mesh	20.07%	-2.86%	29.09%	-3.29%
Exact Numerical	20.66%		30.08%	

Table 6: Comparison of the increases in performance with the exact numerical values.

7. Conclusions

A successful prediction of the integral coefficients for the initial configuration was achieved with the Reynolds-Averaged Navier-Stokes equations, the Menter SST $k-\omega$ turbulence model and the $\gamma - Re_\theta$ transition model. However recommendations for improvements in the definition of the geometry are unavoidable and are of extreme importance for future works.

A sensitivity study of the design parameters, for two wing tip devices, the winglet and the raked tip, was implemented and results showed that for both configurations, the wing tip device's span is the parameter with the most influence in the performance coefficients L/D and $C_L^{3/2}/C_D$. When comparing the inviscid results from the sensitivity study, obtained with panel method simulations, the two wing tip devices prove the tendency presented in section 2. In inviscid flow, the raked tip show higher increases in the performance coefficients than winglets.

An attempt at confirming these increases with the RANS equations was performed and results proved a different tendency. When comparing the results obtained for the winglet, with the RANS

equations, the Menter SST $k-\omega$ turbulence model and the $\gamma - Re_\theta$ transition model, with the results obtained by Panagiotou et al. [5], one can prove that the decrease in drag and consequent increase in performance through the introduction of winglets is not dependent on the turbulence model employed in CFD simulations.

The estimations for the exact numerical values show increases in L/D and $C_L^{3/2}/C_D$ of 20.66% and 30.08%, regarding the cut-off configuration, and 10.51% and 15.26% regarding the initial configuration provided by the Portuguese Air Force.

Acknowledgements

The author would like to acknowledge Major Diogo Duarte of the Portuguese Air Force for the opportunity to develop this paper in cooperation with the Portuguese Air Force. The author would also like to thank Dr. Nelson Marques for receiving him at blueCAPE, Lda and for making the necessary computational infrastructure available.

References

[1] TEAL Group Corporation. *World Unmanned Aerial Vehicle Systems 2011.* 2012.

[2] J. Chow, G. Zilliac, and P. Bradshaw. Mean and Turbulence Measurements in the Near Field of a Wingtip Vortex. 35(10):1561–1567, 1997.

[3] M. D. Maughmer. The Design of Winglets for High-Performance Sailplanes. *AIAA Journal of Aircraft*, 40(6):1099–1106, 2003.

[4] S. A. Ning and I. Kroo. Multidisciplinary Considerations in the Design of Wings and Wing Tip Devices. *AIAA Journal of Aircraft*, 47(2):534–543, 2010.

[5] P. Panagiotou, P. Kaparos, and K. Yakinthos. Winglet design and optimization for a MALE UAV using CFD. *Aerospace Science and Technology*, 39:190–205, 2014.

[6] B. Gunston. *The Cambridge Aerospace Dictionary.* Cambridge University Press, New York, second edition, 2013.

[7] J. Roskam, C. Tau, and E. Lan. *Airplane Aerodynamics and Performance.* 1997.

[8] O. Gur, W. H. Mason, and J. A. Schetz. Full-Configuration Drag Estimation. *Journal of Aircraft*, 47(4):1356–1367, 2010.

[9] I. Kroo. DRAG DUE TO LIFT: Concepts for Prediction and Reduction. *Annual Review of Fluid Mechanics*, pages 587–617, 2001.

[10] R. T. Whitcomb. A design approach and selected wind tunnel results at high subsonic speeds for wing-tip mounted winglets. (July):1–33, 1976.

[11] S. Gudmundsson. *General Aviation Aircraft Design: Applied Methods and Procedures.* Butterworth-Heinemann, Oxford, United Kingdom, 2014.

[12] S. A. Ning and I. Kroo. Tip Extensions , Winglets , and C-wings : Conceptual Design and Optimization. *AIAA Journal*, 26(August):1–33, 2001.

[13] J. Hess. Panel Methods In Computational Fluid Dynamics. *Annual Review of Fluid Mechanics*, 22:255–274, 1990.

[14] J. H. Ferziger and M. Peric. *Computational Methods for Fluid Dynamics.* Springer, New York, third edition, 2002.

[15] P. R. Spalart and S. R. Allmaras. A One-Equatlon Turbulence Model for Aerodynamic Flows. *AIAA paper 1992-0439*, 1992.

[16] F. R. Menter. Improved two-equation k-omega turbulence models for aerodynamic flows. *NASA Technical Memorandum*, (103978):1 – 31, 1992.

[17] R. B. Langtry and F. R. Menter. Transition Modeling for General CFD Application in Aeronautics. *AIAA Journal*, (January):1–14, 2005.

[18] R. Veríssimo. Best Practice Guidelines in CFD External Aerodynamics - Applied to Unmanned Aerial Vehicles at Cruise Conditions. Master's thesis, 2016.

[19] T. C. Corke. *Design of Aircraft.* Pearson Education Limited, Upper Sadle River, 2003.

[20] P. J. Roache. Quantification of Uncertainty in Computational Fluid Dynamics. *Annual Review of Fluid Mechanics*, 29(1):123–160, 1997.